Catalysis Today 171 (2011) 126–131

Contents lists available at ScienceDirect

Catalysis Today

journal homepage: www.elsevier.com/locate/cattod

Catalytic steam reforming of methane under conditions of applicability with Pd membranes over supported Ru catalysts

M.A. Soria[a], C. Mateos-Pedrero[a], I. Rodríguez-Ramos[a,c], A. Guerrero-Ruiz[b,c,*]

[a] Instituto de Catálisis y Petrol., CSIC, Campus Cantoblanco, 28046 Madrid, Spain
[b] UA UNED-ICP(CSIC) Group Des. Appl. Heter. Catal, Spain
[c] Dpto. Química Inorgánica y Técnica, Facultad de Ciencias UNED, Senda del Rey 9, 28040 Madrid, Spain

ARTICLE INFO

Article history:
Received 29 October 2010
Received in revised form 8 February 2011
Accepted 16 February 2011
Available online 21 March 2011

Keywords:
Ru catalysts
Methane steam reforming
Ni/SiO_2
Pd membrane
Deactivation

ABSTRACT

Three Ru catalysts supported on SiO_2, ZrO_2–SiO_2 and ZrO_2–La_2O_3 have been prepared, characterized and tested in the methane steam reforming (SR) reaction, and for comparative purposes a Ni/SiO_2 catalyst has also been studied. Conditions of catalytic studies have been selected for the subsequent application in a hydrogen extraction Pd membrane reactor. That is, reaction temperatures in the range of 400–550 °C and with different amounts of catalyst in order to work under and/or close to the equilibrium conversion conditions. All the supported Ru samples exhibit high catalytic activity and similar CO and H_2 yields. Finally these catalysts are fully stable under reaction conditions at 550 °C for 15 h, while the Ni/SiO_2 sample suffers a significant deactivation. The main deactivation process affecting this latter catalyst is the carbon deposition of partially dehydrogenated intermediates as detected by Raman spectroscopy. Hence, these Ru catalysts appear to be suitable for application combined with metallic (Pd) membrane.
© 2011 Elsevier B.V. All rights reserved.

1. Introduction

Steam reforming (SR) of methane (principal component of natural gas) represents the main commercial route for syngas production. This mixture of H_2 and CO serves as the important intermediate in the gas to liquid technologies. The SR reaction (Eq. (1)) is strongly endothermic and equilibrium limited therefore high reaction temperatures (600–900 °C) are required prior to achieve a sufficient methane conversion. In general, the SR is followed by the water gas shift reaction (WGSR), which is slightly exothermic, as shown by Eq. (2) [1]:.

$$CH_{4(g)} + H_2O_{(g)} \leftrightarrow CO_{(g)} + 3H_{2(g)} \quad \Delta H^\circ = 206.0\,\text{kJ/mol} \tag{1}$$

$$CO_{(g)} + H_2O_{(g)} \leftrightarrow CO_{2(g)} + H_{2(g)} \quad \Delta H^\circ = -41.2\,\text{kJ/mol} \tag{2}$$

The high temperature operation causes strong limitations for the material employed in the reactor, irreversible carbon formation and large energy consumption. One possible way to work at low reaction temperature obtaining higher conversion of methane is to shift the thermodynamic equilibrium by removing hydrogen from the products mixture. This has been done by using reactors that combine steam reforming and hydrogen-permeable membranes [1,2]. These membranes used for the hydrogen separation are mainly based on metallic palladium [3,4]. Furthermore this coupled method can also be interesting to improve the hydrogen yield of the general process, considering the parallel shift of the reaction equilibrium originated by the hydrogen removal from the effluent products.

From the point of view of the SR catalysts, these have to be (i) very active, (ii) capable to work at relatively low reaction temperatures, where the palladium membranes can operate, and (iii) fully stable under reaction conditions.

The most widely used catalysts in the methane SR for the industrial production of H_2 or synthesis gas are nickel based ones. Although catalytically efficient, it is well known that supported Ni catalysts suffer from deactivation by particle sintering and/or by reaction with supports and carbon deposition [5–7]. Noble metals (Ru, Rh, Pd Ir and Pt) are also active for steam reforming. Among them, ruthenium and rhodium have been shown to be the most active catalysts in addition to stable [8–12], but Ru is significantly cheaper. Furthermore, Ru catalyst allows working at low steam to methane ratios without carbon deposition and changing of mechanical properties of the catalyst [13].

There have been a number of studies that have addressed the support effects and it has been shown that the support has limited effect on the activity of the metal for steam methane reforming, provided that the support is alkali-free [5,14]. In the absence of alkali traces the only significant support effect found has been the

* Corresponding author at: Dpto. Química Inorgánica y Técnica, Facultad de Ciencias UNED, Senda del Rey 9, 28040 Madrid, Spain. Tel.: +34 915854765; fax: +34 913986697.
E-mail address: aguerrero@ccia.uned.es (A. Guerrero-Ruiz).

0920-5861/$ – see front matter © 2011 Elsevier B.V. All rights reserved.
doi:10.1016/j.cattod.2011.02.020

variance of metal dispersion on different supports [12]. We have selected support materials, with low metal–support interactions, SiO_2 instead of Al_2O_3, and comparatively a refractory ZrO_2 which is well structurally stabilized either with SiO_2 or with a more basic component as La_2O_3.

Our aim is not only to operate these catalysts under conditions near the thermodynamic equilibrium, where they will be applied in combination with the membrane, in the title catalyzed reaction but also to verify their stability under long term reaction operation.

2. Experimental

2.1. Synthesis of catalysts

Catalysts were prepared using commercial supports: SiO_2 (Silica gel from Fluka), ZrO_2 stabilized with SiO_2 (3.5%) or with La_2O_3 (7.0%) both provided by MEL. Supports were calcined in air at 500 °C for 4 h prior to metal loading. The surface areas of these materials after calcination were 400, 80 and 105 m^2/g for SiO_2, ZrO_2–SiO_2 and ZrO_2–La_2O_3, respectively. The surface of the supports was impregnated with Ru by means of the wetness impregnation method using aqueous solution of $RuCl_3{\cdot}H_2O$ (Sigma–Aldrich) precursor [15]. After Ru impregnation the catalysts precursors were dried in air at 110 °C overnight. In all cases the added metal loading was close to 4 wt.% For comparative purposes, a Ni supported on SiO_2 (Silica gel from Fluka; $Ni(NO_3)_2{\cdot}6H_2O$ from Sigma–Aldrich) was also prepared employing the same synthesis conditions as for the supported Ru samples.

Samples were labelled as Ru/SiO_2, Ru/ZrO_2–SiO_2 and Ru/ZrO_2–La_2O_3 for Ru supported on SiO_2, ZrO_2–SiO_2 and ZrO_2–La_2O_3, respectively. The supported Ni sample was denoted as Ni/SiO_2.

2.2. Characterization

Temperature-programmed reduction (TPR) measurements were carried out in a continuous flow fixed bed reactor operating at atmospheric pressure over 100 mg of sample under a continuous flow at 100 mL/min of a H_2/Ar gas mixture (5 vol.% H_2). The temperature was increased from room temperature to 600 °C with a heating ramp of 8 °C/min. The outlet gas composition was measured by on-line gas chromatography (Varian 3400) with a thermal conductivity detector (TCD) equipped with a Porapaq Q column.

The heats of CO adsorption at 57 °C were measured in a differential heat-flow microcalorimeter (Tian–Calvet type C80 from Setaram). The adsorption vessels were connected to a Pyrex volumetric apparatus equipped with greaseless stopcocks that permitted the introduction of small pulses of CO [16]. The samples were activated in flowing H_2 at 500 °C for 2 h and, after outgassing at this temperature for 16 h, were cooled to the adsorption temperature. Successive doses of CO were then transferred to the sample. The equilibrium pressure was measured by means of a Baratron pressure transducer MKS instrument.

The metal dispersions (D) were calculated from the total CO uptake at the monolayer (N_{ads}), considered to be attained when the evolved heat falls to the physisorption field (≈40 kJ/mol), and assuming a M:CO = 1:1 stoichiometry [17,18]. The initial CO adsorption heats (q^0_{ads}) were determined by extrapolation to zero coverage the chemisorption heat curves obtained from the adsorption microcalorimetric experiments. The average particle sizes of Ru were calculated from dispersion values, assuming spherical metal particles, using the equation d (nm) = 1.32/D [19]. The microcalorimetric profiles that will be shown in the present work represent the variations in the differential CO adsorption heats with the carbon monoxide coverage (θ). The latter is determined as the ratio between the adsorbed amount at a given point and the monolayer uptake (N_{ads}) of the sample. This procedure facilitates comparison of catalysts with different dispersions.

The XPS measurements were performed using an Omicron spectrometer equipped with an EA-125 hemispherical electron multichannel analyzer and a Mg Kα X-ray source having a radiation energy of 1253.6 eV. The samples were slightly pressed into a small pellet of 15 mm diameter, mounted on the sample holder and then introduced into the chamber, where they were outgassed for 6–8 h, in order to achieve a dynamic vacuum below 10^{-8} Pa. The spectra of the samples were registered at 75 W and a pass energy of 20 eV. The electronic state of Ru was characterized by the binding energy of the $3d_{5/2}$ peak. The binding energies were referenced to the C 1s peak (C–C, C–H) of the adventitious carbon set a 284.6 eV. The data were processed with the Casa XPS program (Casa Software Ltd., UK). The peak areas were determined by integration employing a Shirley-type background. Peaks were considered to be a mix of Gaussian and Lorentzian functions in a 70/30 ratio. For the quantification of the elements, sensitivity factors provided by the manufacturer were used.

The Laser Raman (LR) spectra were recorded using a Horiba iHR 320 Jobin Yvon spectrometer equipped with a Synapse CCD detector. Laser radiation (λ = 632.81 nm) was used as excitation source at 5 mW. All measurements were recorded under the same conditions (1 s of integration time and 30 accumulations) using a 100× magnification objective and a 125 μm pinhole.

2.3. Activity measurements

Steam reforming reaction was carried out at atmospheric pressure in a fixed-bed tubular reactor. The reactor with an inner diameter of 11.8 mm was heated in an electric furnace equipped with a programmable temperature controller. A fresh 30 mg catalyst (particle size between 150 and 250 μm) was diluted with SiC to obtain 50 mm bed height and packed in the middle of the reactor. The temperature was monitored by a K-type thermocouple placed in the center of the catalyst bed.Before reaction the catalyst was reduced in situ at 550 °C (maximum operation temperature) during 2 h with a mixture of 25 vol.% H_2 in He at a flow of 100 ml/min. After reduction, He was used during 30 min to sweep the H_2 from the reactor. The feed steam gas mixture consisted of CH_4, H_2O and He with a vol.% ratio CH_4:H_2O:He = 8:8:84. The total flow rate was 100 ml/min (GHSV = 2×10^{-5} ml h^{-1} g^{-1} catalyst). The reactant gases were measured-controlled by mass flowmeters (Brook).

The steam was fed by using a saturator with distillate water into the thermostatic bath. The partial pressure of water was adjusted by controlling the temperature of the bath. The lines before and after reactor were heated (110 °C) to avoid water condensation. Before steam was fed to the chromatograph, water was condensed employing a cool trap. The catalytic activity was measured at 400, 450, 500 and 550 °C.

Gas analyses of both reactants and products were carried out by on line GC (Varian 3400) equipped with a TCD detector (He was used as carrier gas with the TCD). Porapaq Q and Chromosorb 102 columns were used to separate the sample gas (CH_4, H_2, CO y CO_2). Preliminary experiments were performed to verify the absence of diffusion limitation and the inert properties of the supports in given conditions. The carbon balance was close to 100% in all the cases.To analyse the stability, of the catalysts we worked below the thermodynamic equilibrium conversion of methane. The stability study was conducted at 550 °C for 15 h. For the given operating conditions, the thermodynamic equilibrium conversion and products compositions were calculated using the software Aspen HYSYS.

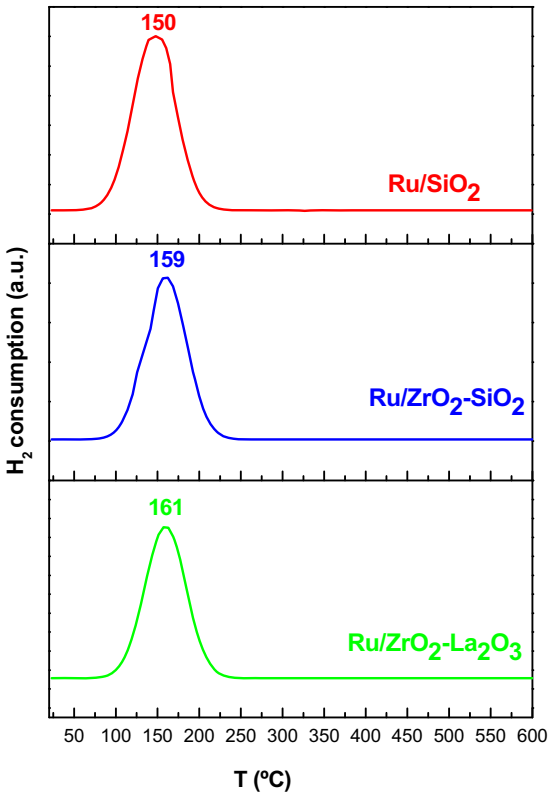

Fig. 1. Temperature programmed reduction profiles of Ru/SiO_2, Ru/ZrO_2–SiO_2 and Ru/ZrO_2–La_2O_3.

The conversion of CH_4 (XCH_4), the yields of CO (YCO) and H_2 (Y_{H_2}) were calculated by means of the following equations:

$$XCH_4\,(\%) = \frac{\text{mols}\,CH_4^{in} - \text{mols}\,CH_4^{out}}{\text{mols}\,CH_4^{in}} \times 100$$

$$YCO\,(\%) = \frac{\text{mols}\,CO^{out}}{\text{mols}\,CH_4^{in}} \times 100$$

$$YH_2\,(\%) = \frac{\text{mols}\,H_2^{out}}{2 \times \text{mols}\,CH_4^{in}} \times 100$$

Catalysts recovered after methane steam reforming measurements performed at various temperatures (activity measurements) will be denoted as "spent catalysts" hereafter.

3. Results and discussion

3.1. Characterization of catalysts

Fig. 1 shows the H_2-temperature programmed reduction profiles for the uncalcined Ru catalysts. At this point, it is important to mention that the catalysts of the present study were not calcined but thermally stabilized by H_2 reduction prior to activity tests, as previously indicated. We have decided to use non calcined catalysts because previous tests performed (under the same operation conditions as those used in the present study) over calcined Ru/SiO_2 samples (under air, 4 h, 550 °C) shown that the catalysts were not active for the SR reaction (results not shown here for the sake of brevity). This is likely owing to the strong interaction Ru-support, which would be favoured during calcination, hindering the reduction of Ru particles and rendering the catalyst inactive for the studied reaction

Table 1
Adsorbed amounts (N_{ads}; μmol/g_{cat}), dispersions (D; %), mean Ru particle sizes (d; nm) and initial adsorption heats parameters assessed from the CO chemisorption experiments for the supported Ru catalysts.

Catalyst	N_{ads} (μmol/g_{cat})	D (%)	d (nm)	q^0_{ads} (kJ/mol)
Ru/SiO_2	62	16	8.4[a]	133
Ru/ZrO_2–SiO_2	112	28	4.7	130
Ru/ZrO_2–La_2O_3	85	24	5.3	127

[a] Mean crystallite size of metallic Ru (Ru/SiO_2) assessed from XRD was 8.9 nm.

Fig. 1 displays the results of the TPR experiments conducted on the uncalcined Ru catalysts. All catalysts exhibit a single and well-defined reduction peak whose maximum lies in the range 150–161 °C. This temperature is well within the range reported for the complete reduction of bulk $RuCl_3$, 160 °C [16,20], which may suggest that these are the main species present on our catalysts.

Based on the TPR data, all catalysts were reduced at temperatures of 500 °C (prior to the activity tests), which has proven to be enough to complete the reduction of the metal precursor ($RuCl_3$) to metallic Ru particles (Ru°).

The CO adsorption amount (N_{ads}), dispersion (D), mean particle size (d) and initial CO adsorption heats (q^0_{ads}) determined from CO chemisorption measurements for the various supported Ru catalysts are given in Table 1. From the data in Table 1 it can be seen that both Ru/ZrO_2–SiO_2 and $Ru\,ZrO_2$–La_2O_3 present nearly the same dispersion (24–28%) and mean particle size (4.7–5.3 nm), but Ru/SiO_2 exhibit a lower dispersion (16%) and consequently higher particle size (8.4 nm).

The CO differential heats for the supported Ru samples are plotted against coverage in Fig. 2. From this figure it is observed that the calorimetric profile of Ru/SiO_2 is different from those of Ru/ZrO_2–La_2O_3 and Ru/ZrO_2–SiO_2. The calorimetric profile of Ru/SiO_2 starts at ca. 133 kJ/mol to gently decrease until reaching a large plateau (~110 kJ/mol) for coverages from 0.2 to 0.65; then, adsorption heats drop to the physisorption region. The constant value over a wide range of surface coverage indicates that an appre-

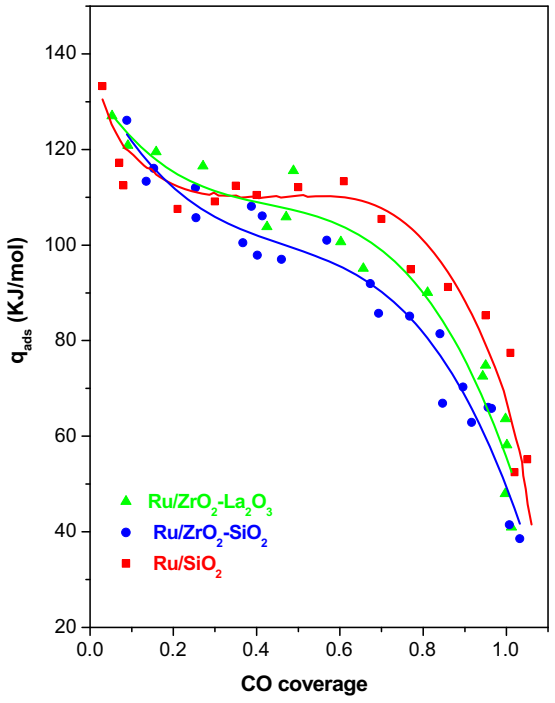

Fig. 2. Differential heats of CO adsorption at 57 °C as a function of surface coverage for supported Ru catalysts reduced at 500 °C: Ru/ZrO_2–La_2O_3 (▲), Ru/ZrO_2–SiO_2 (●) and Ru/SiO_2 (■).

Table 2
$Ru3d_{5/2}$ BE and XPS atomic ratios of the reduced and used supported Ru samples.

Sample	Binding energy (eV)	Surface composition (At. %)	
	$Ru3d_{5/2}$	Ru/Si	Ru/Zr
Ru/SiO_2	280.4	0.009	–
Ru/SiO_2 used	282.9	0.010	–
Ru/ZrO_2–SiO_2	280.9	–	0.05
Ru/ZrO_2–SiO_2 used	282.5	–	0.03
Ru/ZrO_2–La_2O_3	280.6	–	0.08
Ru/ZrO_2–La_2O_3 used	280.8	–	0.11

ciable part of the ruthenium surface centers act homogeneously for the chemisorption of CO, that is, have very similar geometry and energetic of interaction with the CO. In contrast, the calorimetric curves of Ru/ZrO_2–La_2O_3 and Ru/ZrO_2–SiO_2 samples are very similar and show a continuous decline of the adsorption heats (Fig. 2) in the entire coverage range. These s-shaped curves are representative of more heterogeneous surfaces (the CO adsorption heats continuously fall from initial coverages until monolayer formation, ≈40 kJ/mol). It is also inferred from Fig. 2, that the three Ru samples behave similarly (very close adsorption heat values) at low CO coverages (θ ~0.0–0.2) but the adsorption heats are appreciably different for medium and high coverages (above 0.2). Ru/SiO_2 displays higher differential adsorption heat values for these latter (θ > 0.2, Fig. 2).

From Fig. 2, it could be suggested that the strength of surface sites seems to depend on the support and increases in the order: Ru/SiO_2 > Ru/ZrO_2–La_2O_3 > Ru/ZrO_2–SiO_2. Considering that the main difference among the three Ru samples is the support (all they were prepared by the same synthesis method and using the same conditions: precursor, solvent, etc.), this variation could be reasonably attributed to differences in the surface properties of the support.

In general, there is a relationship among CO adsorption heat values and the structure and/or morphology of the metal particles. The values for CO adsorption heats over the different Ru crystallographic planes are given in [21,22], and [references herein]. It is found that CO adsorbed on: Ru(1 0 0 0) or (1 1 0 0), Ru(0 0 0 1) and Ru(1 0 $\bar{1}$ 0) gives adsorption heat values of 105–120 kJ/mol, 160 kJ/mol and 140–150 kJ/mol, respectively. Based on these data, it can be argued that Ru particles in our catalysts expose mainly (1 0 0 0) and (1 1 0 0) crystallographic planes.

On the other hand, differences in the CO adsorption heats can be due to changes in the CO adsorption stoichiometry, as reported in [21] for Ru and Ru-bimetallic samples. In fact, various CO adsorbed species have been detected by FTIR on supported Ru catalysts [23] and [references therein]. Comparison of the present microcalorimetric results with FT-IR of adsorbed CO studies on SiO_2-supported Ru catalysts [24], allows us to suggest the presence of some bridged (Ru_2CO) and linear (Ru–CO) CO species (most of the sites are linear and they are represented by the plateau in the calorimetric profiles of Fig. 2) adsorbed on our supported Ru particles, corresponding to adsorption heat values of ca. 140 and 100–130 kJ/mol, respectively.

The $Ru3d_{5/2}$ binding energies (BE) and the XPS atomic ratios for the various Ru catalysts after reduction and after use in the methane steam reforming reaction are compiled in Table 2.

According to the literature, a BE of $Ru3d_{5/2}$ value in the 279.7–280.2 eV range is assigned to Ru^0 [25,26]. The ruthenium in an oxidation state of Ru^{4+} and Ru^{6+} presents a binding energy close to 280.7 eV and between 282.3 and 282.8 eV for RuO_2 and RuO_3, respectively. The BE of $Ru3d_{5/2}$ exhibits a BE around to 281.8 in $RuCl_3$ [25].

The BE of $Ru3d_{5/2}$ in our reduced catalysts ranges from 280.4 to 280.9 eV (Table 2), which suggests the presence of Ru^0 [25].

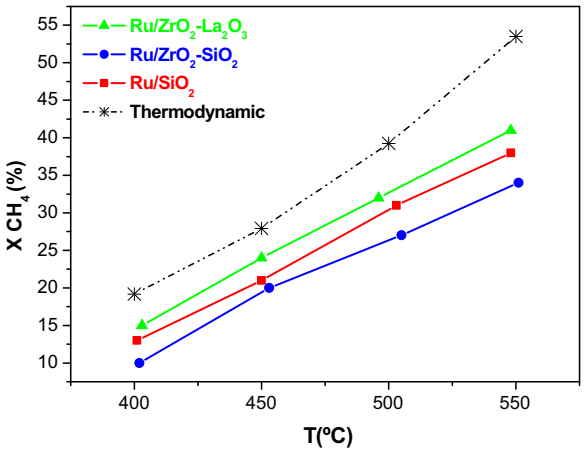

Fig. 3. Methane conversion (%) in the steam reforming reaction as a function of the temperature for Ru/ZrO_2–La_2O_3 (▲), Ru/ZrO_2–SiO_2 (●) and Ru/SiO_2 (■); comparison with thermodynamics.

The presence of these species in the Ru catalysts has been already revealed by TPR experiments. The used Ru/SiO_2 and Ru/ZrO_2–SiO_2 catalysts show a $Ru3d_{5/2}$ BE (282.5–282.9 eV) considerably higher than the reduced ones (Table 2). This value could be reasonably ascribed to Ru^{IV} (RuO_2), in accordance with the values reported for these species [25,27]. The presence of RuO_3 is put aside in this work since this species has not been reported as a solid phase being stable only as a vapour phase from 1200 °C to 1500 °C [27]. The presence of Ru^{IV} species may be derived from either oxidation upon steam reforming reaction or after exposure of used samples to air at room temperature. In the case of the used Ru/ZrO_2–La_2O_3 sample, the binding energy of $Ru3d_{5/2}$ shows almost the same value in relation to the reduced sample (280.6 and 280.8 eV for the used and reduced Ru/ZrO_2–La_2O_3 sample, respectively; Table 2). This fact suggests that Ru particles do not undergo further oxidization during reaction and supports the above second attribution.

The C1s spectra for the various Ru catalysts showed one peak centered at 284.6 eV (belonging to adventitious carbon), no other peaks were observed. On the other hand, the C amount detected over the samples before and after SR reaction remains unchanged. This indicates that no coke deposits measurable by XPS were formed on our Ru catalysts during SR reaction. The XPS atomic ratios for the reduced and spent Ru samples are given in Table 2. As it can be seen, for the spent catalysts the surface atomic ratios were not appreciably modified in comparison with the catalysts before reaction (reduced samples), suggesting that no significant change in the dispersion occurred.

In summary, the data provided by the characterization pointed out the great resemblance of the three supported Ru samples in terms of reducibility, Ru dispersion and particle size.

3.2. Activity in the methane steam reforming (SR) at low temperature

3.2.1. Activity measurements

Fig. 3 shows the reforming activities of the catalysts in terms of methane conversion (%) in the steam reforming reaction as a function of the temperature (from 400 to 550 °C; this temperature range has been explored because it is the temperature interval applicable in the membrane reactor). Methane conversions predicted by thermodynamics are also included in this figure, for comparison. The three catalysts show a similar trend, that is, the increase of the reaction temperature results in enhancing the activity, in accordance with thermodynamics predictions. On the other hand, all the supported Ru samples present comparable conversion values at given

Table 3
Comparative of the methane steam reforming catalytic results over the supported Ru catalysts.

Catalysts	T (°C)	CH_4 converted (μmol/s g_{cat})	Y_{H_2}	YCO	YCO_2	H_2/CO ratio
Ru/SiO_2	400	32.2	26	1	12	52.0
	450	52.1	37	4	17	19.0
	500	76.8	51	13	18	9.0
	550	94.2	59	24	14	6.0
Ru/ZrO_2–SiO_2	400	24.8	21	1	9	53.0
	450	49.6	35	5	16	20.0
	500	66.9	47	11	17	9.0
	550	84.3	52	19	15	6.0
Ru/ZrO_2–La_2O_3	400	37.2	27	1	15	47.0
	450	59.5	41	4	20	19.0
	500	79.3	52	12	20	10.0
	550	101.6	63	24	17	6.0

temperature (Fig. 3). As a minor observation, Ru/ZrO_2–SiO_2 exhibits the lowest activity among the analyzed catalysts.

In Table 3 are shown, for various reaction temperatures, methane catalytic conversions (expressed as μmol of CH_4 converted per gram of catalyst and per second) and the yield to H_2 (Y_{H_2}) and CO (Y_{CO}) obtained over the three prepared catalysts. The H_2 to CO molar ratio are also reported in this table. As already mentioned in Section 2.3, different masses of catalysts were evaluated in order to approach the thermodynamic equilibrium. Table 3 data correspond to the tests performed with a minimal amount catalyst (30 mg), in such conditions we can be sure to operate under non-equilibrium conditions.

It is observed that the increase of the reaction temperature originates an improvement in the CH_4 conversion, and yields both for H_2 and for CO (Table 3). However, in agreement with thermodynamic predictions, in the range of explored temperatures the selectivity to CO increases in a higher extension, as can be seen in the latter column of this table (H_2/CO ratio). On the other hand, the variation of CO_2 yield with reaction temperature (Table 3) shows the same trend over the three studied catalysts. It increases steadily with the reaction temperature and reaches a maximum at about 500 °C, then decreases gradually with further increase in temperature. The modifications in selectivity/yield with the reaction temperatures can be explained assuming that the water gas shift reaction ($H_2O + CO \rightarrow H_2 + CO_2$) is favoured at lower temperatures, which is also in agreement with the reaction thermodynamic predictions. Finally, all supported Ru catalysts give place to similar selectivity values and the obtained catalytic activities are quite close.

To sum up, the three supported Ru catalysts evaluated in this work exhibit a similar catalytic behaviour in terms of methane SR reaction, consistent with the similarities in dispersion and Ru particle size shown by these catalysts, as revealed the characterization. These results agree with earlier studies which pointed that non-reducible supports have limited effect on the activity of metal catalysts for methane steam reforming [11].

3.3. Stability measurements

It is very important to test the stability of the supported Ru catalysts on the one hand, considering the endothermic character of this reaction and the relatively high temperatures of operation and, on the other hand, that one of our objectives is to test catalytic performance of these Ru samples for its posterior utilisation in a Pd membrane reactor. On this sense, the stability of the catalysts becomes of paramount importance in order to avoid the membrane damage. With this aim, some tests were conducted at 550 °C for 15 h. In these cases the catalyst amounts in the reactor were minima (30 mg of sample). These results are reported in Fig. 4. It should be noticed that the three studied catalysts do not modify significantly the methane conversion (neither the product yields), i.e. all they are quite stable. This fact becomes even more evident from Fig. 5, where the effect of time on stream on the activity of Ni and Ru supported samples is compared. As shown in Fig. 5, initially both catalysts show comparable activities (although the Ru based catalyst is somewhat more active, 37 vs. 30% for Ru and Ni supported samples, respectively), but the most important aspect to be noticed is that the Ni catalyst suffered strong deactivation during the first 2 h of reaction. In fact, the activity of Ni/SiO_2 dramatically decays, after only 90 min on stream, demonstrating its instability, whereas the Ru/SiO_2 sample did not show significant deactivation (57% vs. 4% of activity loss for Ni and Ru supported samples, respectively).

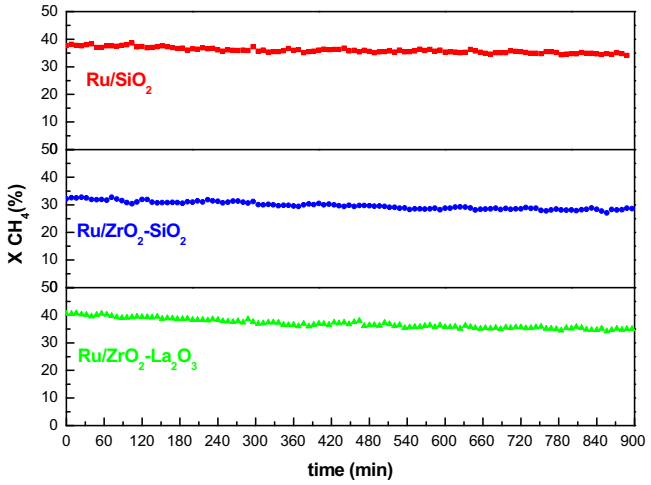

Fig. 4. Methane conversion (%) versus time on stream during SR reaction at 550 °C over supported Ru catalysts; Ru/ZrO_2–La_2O_3 (▲), Ru/ZrO_2–SiO_2 (●) and Ru/SiO_2 (■).

Laser Raman (LR) spectroscopy was employed to detect carbon deposits in the catalysts after steam reforming reaction. The LR spectra of Ru/SiO_2, Ru/ZrO_2–SiO_2 and Ni/SiO_2 samples are shown in Fig. 6. The LR spectrum of Ni/SiO_2 sample have bands at 1340 (D mode) and 1580 cm^{-1} (G mode). The band at 1580, named the G peak, is the E2g mode of bulk graphite; its intensity increases with the crystal size. The band at 1340, designated as D peak, was assigned to the analogue of the E2g mode for the edges of the graphite layers and is closely related to the disorder-induced scattering resulting from imperfections [28]. Clearly, LR results show that significant carbon deposition occurred in the case of Ni/SiO_2

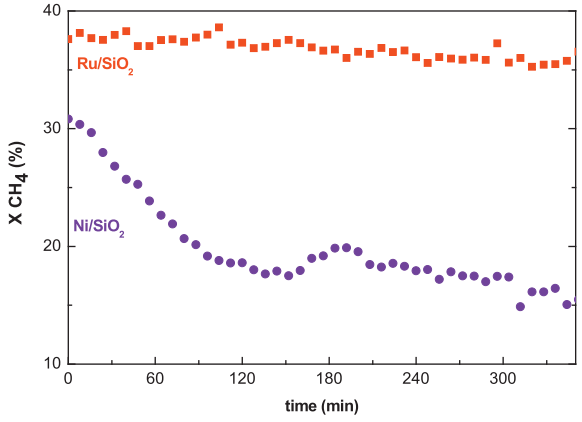

Fig. 5. Effect of time on stream on the catalytic activity of Ni/SiO_2 (7 wt.% Ni; ●) and Ru/SiO_2 (4 wt.% Ru; ■) at 550 °C.

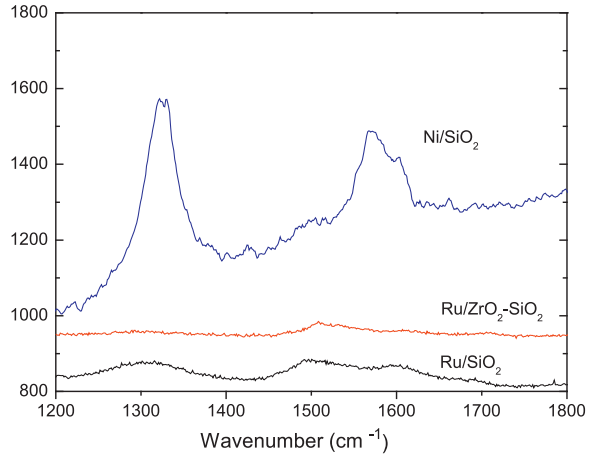

Fig. 6. Raman spectra for catalysts recovered after steam methane reaction at 550 °C for 15 h.

catalyst. It could be concluded that the activity loss of Ni/SiO_2 catalyst during the SR reaction was caused by carbon deposition. However, the LR spectra of ruthenium samples after reaction show very poor features due to carbon deposited on the catalysts. The small amount of carbon deposits detected by LR seems to be probably located on the support surfaces as no effect was observed on the catalyst activity. In addition, no carbon was detected through XPS measurements carried out on the used ruthenium catalysts. In agreement with the presence of only traces of carbon (if any) is the fact that no deactivation of the catalysts was observed after stability tests (Fig. 4). Interestingly, this is contrary to that reported by Jones et al. [11]. They observed in SR tests with Ru on Al_2O_3 and ZrO_2 catalysts, a significant loss in activity at 550 °C and above for catalyst grain sizes smaller than 300 μm. Based on this finding they justify their chosen catalyst particle size (300–500 μm). However, our results are in the line of the previously reported for Ru/Al_2O_3 catalysts [10]. Finally the findings of the present contribution constitute an important result for our further purpose of identifying enough active and stable SR catalysts for Pd membrane reactors.

4. Conclusions

The three Ru-containing catalysts studied here are active for the steam reforming of methane, and very stable for at least 15 h on stream, and only form traces of graphitic carbon detected by LR spectroscopy. All these catalysts appear to be very stable in SR under membrane operation conditions. Contrarily Ni/SiO_2 catalyst suffers deactivation and carbon deposits have been evidenced by LR.

As conclusion we have some very promising catalysts to be applied inside membrane operation systems. In following steps, we have to evaluate the Ru catalysts in a multifunctional membrane reactor but also the combination of SR with dry reforming and water gas shift reactions.

Acknowledgement

Authors acknowledge the MICINN of Spain (projects CTQ-2008-06839-C03-01 and 03-PPQ, CTQ 2008-03068-E/PPQ and CIT-120000-2008-4) for the financial support.

References

[1] L. Barelli, G. Bidini, F. Gallorini, S. Servili, Energy 33 (2008) 554–570.
[2] G.Q. Lu, J.C. Diniz da Costa, M. Duke, S. Giessler, R. Socolow, R.H. Williams, T. Kreutz, J. Colloid Interface Sci. 314 (2007) 589–603.
[3] Y. Matsumura, J. Tong, Top. Catal. 51 (2008) 123–132.
[4] A. Criscuoli, A. Basile, E. Drioli, Catal. Today 56 (2000) 53–64.
[5] J.R. Rostrup-Nielsen, J. Sehested, J.K. Nørskov, Adv. Catal. 47 (2002) 65–139.
[6] Y. Matsumura, T. Nakamori, Appl. Catal. A: Gen. 258 (2004) 107–114.
[7] T. Borowiecki, W. Gac, A. Denis, Appl. Catal. A: Gen. 270 (2004) 27–36.
[8] J.R. Rostrup-Nielsen, J.-H.B. Hansen, J. Catal. 144 (1993) 38–49.
[9] E. Kikuchi, S. Tanoka, Y. Yamazaki, Y. Morila, Bull. Jpn. Pet. Inst. 16 (1974) 95–101.
[10] J.M. Wei, E. Iglesia, J. Phys. Chem. B 108 (2004) 7253–7262.
[11] G. Jones, J.G. Jakobsen, S.S. Shim, J. Kleis, M.P. Andersson, J. Rossmeisl, F. Abild-Pedersen, T. Bligaard, S. Helveg, B. Hinnemann, J.R. Rostrup-Nielsen, I. Chorkendorff, J. Sehested, J.K. Nørskov, J. Catal. 259 (2008) 147–160.
[12] J.M. Wei, E. Iglesia, J. Phys. Chem. B 108 (13) (2004) 4094–4103.
[13] A. Berman, R.K. Karn, M. Epstein, Appl. Catal. A: Gen. 282 (2005) 73–83.
[14] R. Craciun, B. Shereck, R.J. Gorte, Catal. Lett. 51 (3–4) (1998) 149–153.
[15] P. Ferrerira, C. Márquez-Alvárez, I. Rodríguez-Ramos, Y. Schuurman, A. Guerrero-Ruíz, C. Mirodatos, J. Catal. 184 (1999) 202–212.
[16] A. Guerrero-Ruíz, P. Badenes, I. Rodríguez-Ramos, Appl. Catal. A: Gen. 173 (1998) 179–187.
[17] E. Miyazaki, J. Catal. 65 (1980) 84–94.
[18] T. Narita, H. Miura, K. Sugiyama, T. Matsuda, R.D. González, J. Catal. 103 (1987) 492–495.
[19] J.R. Anderson, Measurement techniques: surface area, particle size and pore structure, in: Structure of Metallic Catalysts, Academic Press, New York/London, 1975, pp. 289–394.
[20] P.G.J. Koopman, A.P.G. Kieboom, H. van Bekkum, React. Kinet. Catal. Lett. 8 (1978) 389–393.
[21] M. Cerro-Alarcón, A. Maroto-Valiente, I. Rodríguez-Ramos, A. Guerrero-Ruiz, Appl. Catal. A: Gen. 275 (2004) 257–269.
[22] A. Maroto-Valiente, M. Cerro-Alarcón, A. Guerrero-Ruiz, I. Rodríguez-Ramos, Appl. Catal. A: Gen. 283 (2005) 23–32.
[23] K. Hadjiivanov, J.C. Lavalley, J. Lamotte, F. Maugé, J. Saint-Just, M. Che, J. Catal. 176 (1998) 415–425.
[24] J.M. Hill, R. Alcala, R.M. Watwe, J. Shen, J.A. Dumesic, Catal. Lett. 68 (2000) 129–138.
[25] D. Briggs, M. P. Seah, Practical Surface. Analysis, vol. 1, second ed., John Willey & Sons 1990.
[26] J.F. Moulder, W.M. Stickle, P.E. Sobol, K.D. Bomben, in: Jill Chastain (Ed.), Handbook of XPS, Perking-Elmer Corporation, Minnesota, 1992.
[27] J.L. Gomez de la Fuente, F.J. Pérez-Alonso, M.V. Martínez-Huerta, M.A. Peña, J.L.G. Fierro, S. Rojas, Catal. Today 143 (2009) 69–75.
[28] A. Cuesta, P. Dhamelincourt, V. Laureyns, A. Martínez-Alonso, J.M.D. Tascón, Carbon 32 (1994) 1523.